ACS APPLIED MATERIALS & INTERFACES

Research Article

www.acsami.org

Sonogashira Couplings on the Surface of Montmorillonite-Supported Pd/Cu Nanoalloys

Wei Xu, Huaming Sun, Bo Yu, Guofang Zhang, Weiqiang Zhang,* and Ziwei Gao*

Key Laboratory of Applied Surface and Colloid Chemistry MOE, School of Chemistry and Chemical Engineering, Shaanxi Normal University, Xi'an 710062, China

Supporting Information

ABSTRACT: To explore the true identity of palladium-catalyzed Sonogashira coupling reaction, montmorillonite (MMT)-supported transition metal nanoparticles (MMT@M, M = Pd, Cu, Fe, and Ni) were prepared, characterized, and evaluated systematically. Among all MMT@M catalysts, MMT@Pd/Cu showed the highest activity, and it was successfully extended to 20 examples with 57%−97% yields. The morphology characterization of MMT@Pd/Cu revealed that the crystalline bimetallic particles were dispersed on a MMT layer as nanoalloy with diameters ranged from 10 to 11 nm. In situ IR analysis using CO as molecular probe and XPS characterization found that the surface of Pd/Cu particles consisted of both catalytic active sites of Pd(0) and Cu(I). The experiments on the catalytic activities of MMT@M found that Pd/Cu catalyst system exhibited high activity only in nanoalloy form. Therefore, the Pd/Cu nanoalloy was identified as catalyst, on which the interatom Pd/Cu transmetalation between surfaces was proposed to be responsible for its synergistic activity.

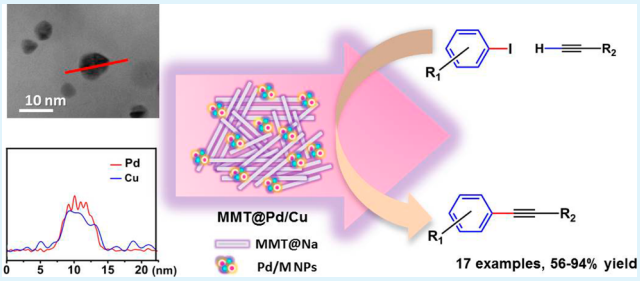

KEYWORDS: *bimetallic catalysis, nanoalloy, montmorillonite, Sonogashira coupling, CO absorption*

1. INTRODUCTION

Bimetallic nanoparticles (NPs) of transition metals have shown superior activity over their monometallic counterparts in many organic transformations.[1−3] Due to the ubiquitous catalytic application of palladium, Pd/M nanoparticles have been devised as a large number of heterogeneous catalysts with excellent selectivity and activity.[4−8] For example, Pd/Au nanoparticles efficiently catalyzed a large number of oxidation reactions,[9] Pd/Pt catalysts were employed as effective catalyst for fuel cells,[10−12] and Pd/Cu[13] or/Ag[14−16] catalysts are widely used in the reduction of oxygen and selective hydrogenation. To further tune the catalytic activity, many researchers have focused on the morphology and size distribution of these nanoparticles. The surface structures of palladium bimetallic catalysts have rarely been investigated,[17,18] although the surface composition of a catalyst is essential for understanding the corresponding catalytic activity.

Palladium and CuI cocatalyst have been successfully applied for Sonogashira coupling reactions in which two cooperative catalytic cycles of Pd and Cu were accepted as a plausible mechanism.[19] While various Pd/Cu catalysts have been developed for this Csp−Csp^2 cross-couplings successfully, the true catalytic active species of Pd/Cu has been argued for years.[20] To illustrate the possibility of bimetallic nanoparticle as real catalyst, herein, we reported the surface structures and the activities of montmorillonite (MMT)-supported bimetallic catalysts. The morphology and size distribution of the materials were examined with high-resolution scanning electron microscope (HR-SEM) fitted with a backscattered electron detector (BSED), high-resolution transmission electron microscope (HR-TEM) and the corresponding selected-area electron-diffraction pattern (SAED), simultaneously. The elemental distributions were investigated by transmission electron microscopy energy-dispersive X-ray spectroscopy (TEM-EDS) line scan. Valence of metals was determined by X-ray photoelectron spectroscopy (XPS). Specifically, the chemical state and composition of nanoparticle surface was studied using the in situ infrared Fourier transform spectroscopy of CO absorption. These results revealed bimetallic particles formed on the surface of natural clay, which were close to nanoscale metal alloys, different from "mixed monometallic nanoparticles" and "core-shell structure".[21] In the Sonogashira reactions, altering the metallic composition of the MMT catalysts changed their catalytic activities significantly.[22] MMT@Pd/Cu exhibited superior activity over MMT@Pd/Fe, MMT@Pd/Ni, and the mixture of MMT@Pd and MMT@Cu. These experimental results clearly demonstrate that the Pd/Cu bimetallic nanoparticles were real catalytic species in the Sonogashira coupling reaction. To the best of our knowledge, nanoalloy surfaces have not been reported as active sites for catalyzed Csp−Csp^2 cross-coupling reactions.

Received: August 27, 2014
Accepted: October 15, 2014
Published: October 15, 2014

Scheme 1. Preparation of Pd-Based MMT Supported Bimetallic NPs

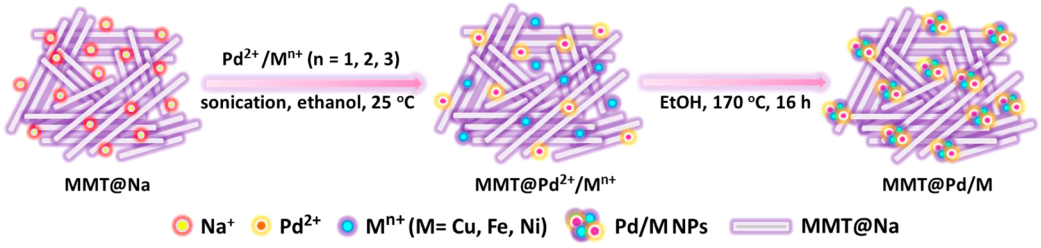

2. EXPERIMENTAL SECTION

The morphology and size distribution of the materials were examined with HR-SEM fitted with a BSED (Figure 1) and TEM (Figure 3; Figures S1 and S4, Supporting Information). HR-SEM was carried out in a JSM-7800F high-resolution TEM (Figure 4). HR-TEM and its corresponding SAED (Figure 5) were examined in a JEOL JF-2100 high-resolution TEM at 200 keV. The structures of monometallic and bimetallic nanoparticles were investigated by X-ray diffraction (XRD) (Figure 2; Figure S5, Supporting Information) using Rigaku D/Max-3BX, and the operating parameters are as follows: monochromatic Cu Kα radiation, Ni filter, 40 mA, 40 kV, 2θ values between 5° and 80°. Surface morphology analyses were carried out by XPS (Figures S8–S11, Supporting Information) using a Kratos AXIS-165 surface analysis system with a monochromatic Al Kα radiation as the excitation source. Collected XPS spectra were analyzed using CasaXPS. All spectra were calibrated using the adventitious C 1s peak with a fixed value of 284.6 eV. In situ FT-IR spectra (Figure 7; Figures S6–S8, Supporting Information) were recorded on a Bruker TENSOR27 spectrometer using a KBr comb.

2.1. Preparation of MMT@Pd/M (M = Cu, Fe, Ni). $Pd(OAc)_2$ (0.0170 g, 0.78 mmol), $Cu(NO_3)_2$ (0.0148 g, 0.78 mmol), and 1.0 g MMT@Na were added into a hydrothermal reactor (30 mL), followed by the addition of ethanol (12 mL). The resulting mixture was vigorously stirred for 30 min and then sonicated for 30 min to promote the ion exchange process between the interlayer Na^+ cations and transition metal cations. After that, the reactor was sealed and heated at 170 °C for 16 h. The reaction mixture was cooled to room temperature and washed with ethanol (3 × 150 mL) three times. The suspension was separated by centrifuge, and the dark brown MMT@Pd/Cu catalyst was obtained after drying in vacuum for 24 h at 25 °C. We used $Fe(NO_3)_2$ or $Ni(NO_3)_2$ substituted for $Cu(NO_3)_2$ to prepare the corresponding MMT-supported bimetallic catalysts in the same fashion.

2.2. In Situ FT-IR Spectra of CO Adsorbed on MMT-Supported Transition Metals. MMT@M (M = Pd, Cu) (1.0 g) was pressed into a self-supporting disk (diameter = 18.0 mm). After the treatment under vacuum at 150 °C, the major surface metal centers, and CO absorption (0.1 Pa equilibrium pressure pulse injected into the reactor) was then monitored by in situ IR technique. Figures S11–S13 (Supporting Information) show the infrared spectra of CO adsorbing on monometallic samples of MMT@Pd, MMT@Cu, and MMT@Pd/Cu.

2.3. MMT@Pd/M (M = Fe, Ni, Cu) Catalyzed Sonogashira Coupling. MMT@Pd/Cu (0.1040 g, Pd 1 mol %), PPh_3 (0.0080 g, 2 mol %), and K_2CO_3 (0.1380 g, 2 mmol) were added into a Schlenk tube (50 mL) and protected by N_2 (5 bar). Dry ethanol (5 mL) was transferred to the mixture via cannula. Iodobenzene (112 μL, 1 mmol) and phenylacetylene (216 μL, 2 mmol) were added dropwise by syringe. The reaction mixture was stirred at 65 °C overnight. After the solvent was removed under vacuum, the crude product was purified by flash column chromatography. The characterization data and copies of spectra are presented in the Supporting Information.

3. RESULTS AND DISCUSSION

3.1. Preparation and Characterization of MMT-Supported Bimetallic Nanoparticles. In previous work, we found that metal salts can be reduced by DMF in the thermal solvolysis reaction system and deposited as nanoparticles on MMT. This kind of nanoparticle showed high activity in the Sonogashira cross-coupling reactions.[23] However, the surface structure analysis revealed that the metallic nanoparticles were composed of palladium, while copper(I) cation was just absorbed by the surface of clay. Herein, to obtain the mixed metallic nanoparticle, we screened the solvent for the solvothermal process because the solvent is crucial for the exfoliation of clay and the sequential reduction of metal precursors. Notably, we found the ethanol is the best media for the preparation of bimetallic-supported MMTs. Transition metals (Cu, Pd, Ni, and Fe) were efficiently deposited on the surface of MMT@Na as bimetallic nanoparticles via an efficient one-pot solvothermal process (Scheme 1), in which alcoholic solvent not only exfoliates MMT layers to enhance the cation exchange, but also facilitates the reduction of the transition metal ions.

The MMT-supported monometallic and bimetallic catalysts were primarily characterized with high-magnification SEM fitted with a BSED and XRD. As shown in Figure 1a, the layer

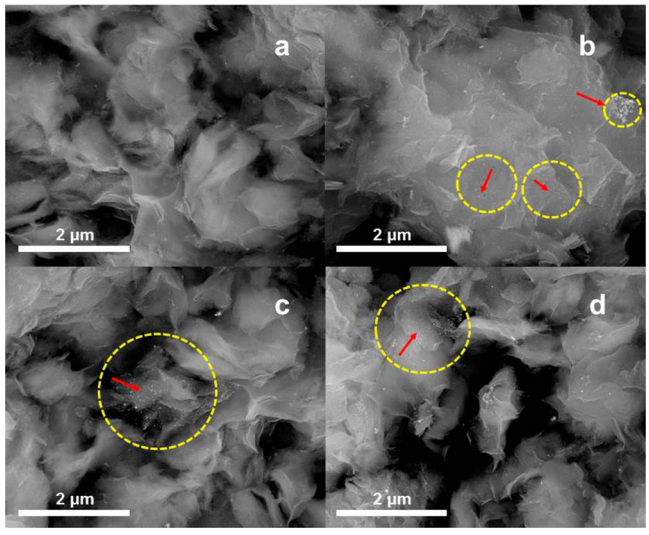

Figure 1. High-magnification SEM images of MMT supported Pd/M (M = Cu, Fe, Ni) particles: (a) MMT@Na, (b) MMT@Pd/Cu, (c) MMT@Pd/Fe, and (d) MMT@Pd/Ni. The high-magnification SEM was fitted with a BSED.

morphology of MMT@Pd/M (M = Cu, Fe, Ni; Figure 1b,c) was identical to MMT@Na, indicating that the layer structures of MMT were intact during the thermal solvolysis preparation of bimetallic nanoparticles and that Pd/M (M = Cu, Fe, Ni) particles were deposited along with the surface of the MMT layers. To further verify the microstructure of MMT@Pd/M

(M = Cu, Fe, Ni), wide-angle powder XRD analysis was carried out (Figure 2).

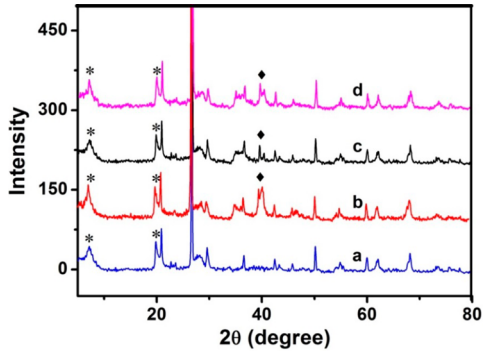

Figure 2. XRD of MMT-supported Pd/M (M = Cu, Fe, Ni) species: (a) MMT@Na, (b) MMT@Pd/Cu, (c) MMT@Pd/Ni, and (d) MMT@Pd/Fe. (*) Diffraction of SiO_2 in MMT and (♦) diffraction of Pd in MMT@Pd/M.

All samples showed well-developed (001) Bragg reflections at $2\theta = 20.1°$, which indicated that such clay material maintains good crystallinity.[24] In Figure 2b, the characteristic diffraction of Pd(111) shifts to $2\theta = 41°$ which was slightly different from the reported value (Pd(111) $2\theta = 40.1°$).[25] It can be concluded that palladium bimetallic species formed, rather than a physical mixture of monometallic particles deposited on MMT. The similar diffraction changes of MMT@Pd/M (Fe, Ni) were observed for the 2θ of Pd(111) (Figure 2c,d), which indicated that the precursors of Fe and Ni might form bimetallic species with Pd.

The morphology and distribution of grown M (M = Pd, Cu, Fe, Ni) nanoparticles on MMT were characterized by TEM. Bright-field TEM images (Figure 3a–d) showed a large amorphous region between spherulites and darker regions inside the spherulite, and in the peripheral region were lamellar structures. As shown in Figure 3, nanoparticles were well dispersed, while clear and clean MMT layers were also observed. By counting more than 1000 NPs, we also obtained a diameter distribution, as shown in Figure 3e–h, where the diameter distribution in histogram gave rise to a diameter of three different NPs. It revealed that the average diameter of the monometallic NPs (Figure 3h; Pd, 13.7 nm) was relatively larger than the bimetallic NPs (Figure 3e–g). The average diameter of Pd/Cu NPs was 10.4 nm, close to the monodisperse distribution,[26] while the average diameters of Pd/Fe NPs and Pd/Ni NPs were 11.3 and 11.8 nm, respectively.

To identify the composite of bimetallic NPs in a single nanoparticle, we investigated the elemental distribution of MMT@Pd/M by TEM-EDS line scan. As shown in Figure 4a,d, the line scan consistently rose and fell as Pd and Cu signals moved along a single particle. This demonstrated that Pd and Cu were present over the entire width of the particle, and neither Pd nor Cu was limited to a narrow region near the particle center. These results suggested that individual particles are not composed of single metal as a core or a shell. It can be concluded that the Pd/Cu particle is a bimetallic alloy structure in nanoscale. In Figure 4b,c, although the signals of Ni and Fe were weaker than the signal of Pd, similar results demonstrated that the Pd/M alloy prepared through the same route contained single phase rather than phase-separated particles

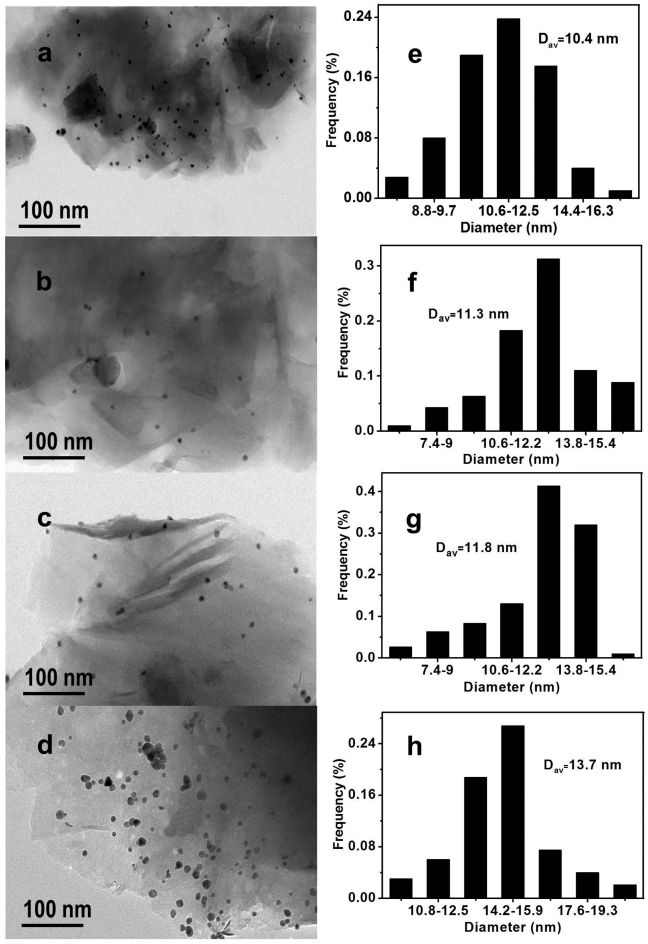

Figure 3. TEM images of MMT supported Pd/M (M = Cu, Fe, Ni) particles: (a) MMT@Pd/Cu, (b) MMT@Pd/Fe, (c) MMT@Pd/Ni, and (d) MMT@Pd. Distributions of (e) Pd/Cu, (f) Pd/Ni, (g) Pd/Fe, and (h) Pd.

with localized Pd and M domains. The low concentration of Fe and Ni might result from high redox potential of these metals. The elemental composition of MMT@Pd/M catalysts was also analyzed by EDS, and the spectra are shown in Table S1 (Supporting Information). MMT@Pd/Cu consisted of Si/Al/O in the ratio of 3:1:4, indicating a intact MMT layers, while Pd/Cu existed in the ratio approximately 1:1. Similar elemental compositions of MMT@Pd/Fe and MMT@Pd/Ni were observed.

To get insight into the structure of these NPs, we characterized the crystalline structures of individual nanoparticles by HR-TEM and the corresponding SAED pattern, simultaneously (Figure 5). In these images, the orientations of the nanocrystallites were determined by the comparison of the features on the diffraction pattern with the local morphology by bright-field image (Figure 5a–c). As shown in Figure 5a–c, the high-magnification TEM images of Pd/M (M = Cu, Fe, Ni) particles revealed that each of the particles was a high-quality nanocrystal with clear lattice fringes. According to the SAED of bimetallic nanoparticles (Figure 5d–f), Pd/Cu, Pd/Fe, and Pd/Ni showed many diffraction rings, and the decreased signal indicated that the polycrystalline structures formed on the surfaces of the MMT layers. On the other hand, Figure 5a shows that two kinds of lattice spaces were measured to be 0.21 and 0.16 nm, as labeled in the image, which were smaller than

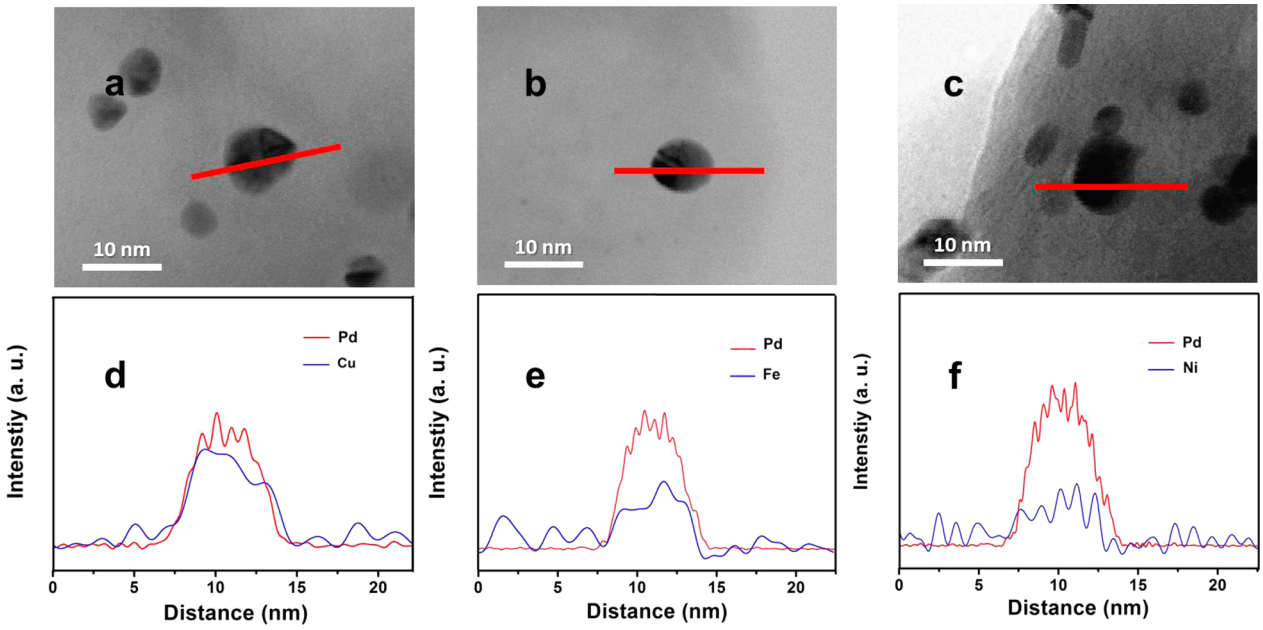

Figure 4. TEM-EDS of MMT supported Pd/M (M = Cu, Fe, Ni) particles: (a) MMT@Pd/Cu, (b)MMT@Pd/Fe, (c) MMT@Pd/Ni. TEM-EDS line scan analyses: (d) line analysis along the line in panel a, (e) line analysis along the line in panel b, and (f) line analysis along the line in panel c.

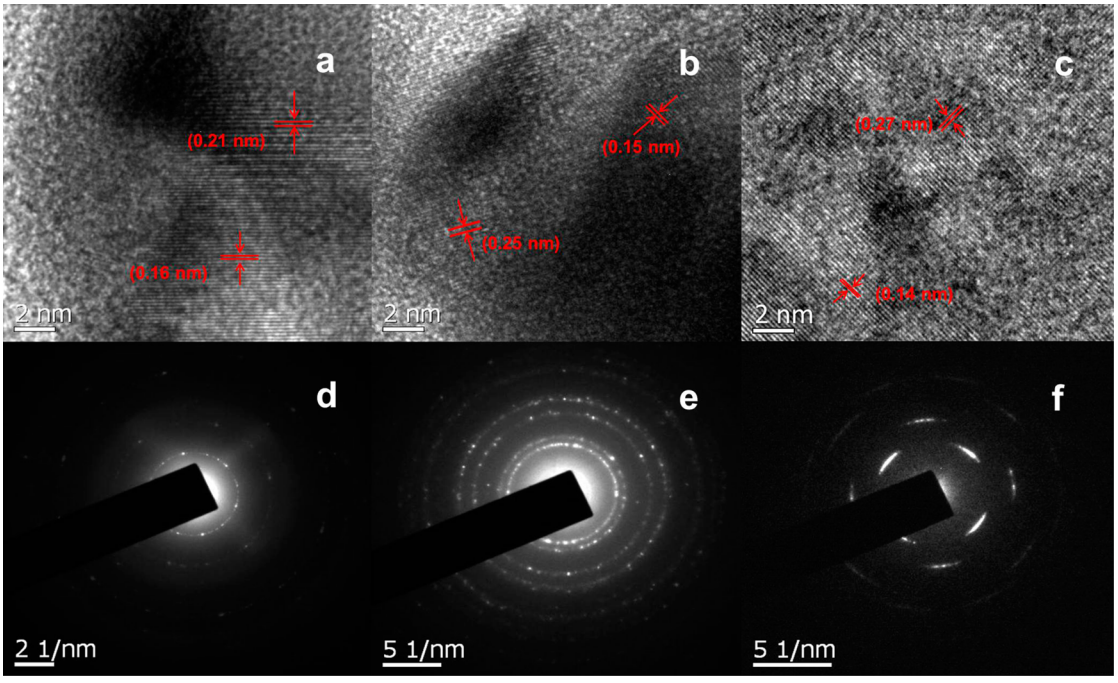

Figure 5. High-magnification TEM images of Pd/M (M = Cu, Fe, Ni) particles and corresponding SAED patterns: (a and d) Pd/Cu, (b and e) Pd/Ni, and (c and f) Pd/Fe.

those of pure Pd(111) plane (0.2265) and Pd(100) (0.1961 and 0.1945 nm) but larger than those of pure Cu(111) (0.2088 nm) and Cu(100) (0.1808 nm). These results implied the formation of Pd/Cu alloy.[27] Similar results are shown in Figure 5b; two different lattice were measured at 0.25 and 0.15 nm. The values were larger than those of pure Pd(111) and Pd(100) and smaller than those of pure Ni(100) and Ni(200). These results indicate that Pd/Ni was also formed with the alloy. Figure 5c also showed two different lattice measured to be 0.27 and 0.14 nm, which were larger than the pure Fe(110) (0.201 nm) and Fe(200) (0.143 nm) and smaller than both the pure Pd(111) plane (0.2265) and Pd(100) (0.1961 and 0.1945 nm), indicating that Pd/Fe were also formed with the alloy. In these SAED images, we can confirm that the copper has (111), (200), and (220) planes (PDF 65−9743) in the Pd/Cu NPs, and the SAED results related to the Pd/Fe bimetallic NPs present the plane (PDF 01−1267) of Fe at (110), (200), and (211), while the Pd/Ni exists the plane (PDF 01-1272) of Ni at (100), (200), and (110).

3.2. Catalytic Activity and Application of MMT@M Catalysts. We evaluated the activity of MMT@M catalysts in the cross-coupling reactions of phenylacetylene and iodoben-

zene under the optimal conditions (Scheme 2; Table S3, Supporting Information). The results of the catalytic reactions

Scheme 2. MMT@M (M = Pd, Cu, Fe, Ni) Catalyzed Sonogashira Cross-Coupling

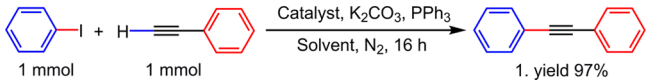

are listed in Table 1. To our surprise, MMT@Pd NPs afforded only 32% yield (Table 1, entry 1), while MMT@Cu gave 40% yield (Table 1, entry 2). None of the MMT@M and MMT@Pd/M (Fe, Ni) catalyzed the cross-coupling efficiently, which gave 6−28% yields (Table 1, entries 3−6). Notably, MMT@Pd/Cu afforded 97% yield (Table 1, entry 7), which was much higher than other MMT@M catalysts, indicating nanoalloy of Pd and Cu might be the true catalytic species. Three kinds of designed mixed metallic catalyst were studied in the reaction (Table 1, entries 8−10). The bimetallic catalyst systems of MMT@Pd/CuI, MMT@Cu/Pd(OAc)$_2$ gave 30 and 10% yields, respectively (Table 1, entries 8−9). No synergistic acceleration effect was observed using the mixture of MMT@Pd and MMT@Cu (Table 1, entry 10). It can be rationalized that under the mild catalytic reaction condition, these metallic precursors unlikely form catalytic active Pd/Cu nanoalloy. These results clearly demonstrated that the formation of Pd/Cu alloy is crucial for the Sonogashira coupling reactions catalyzed by MMT@M.

Furthermore, the scope and limitations of MMT@Pd/Cu catalyst were investigated in Sonogashira coupling reactions (Table 2). The cross-couplings of aliphatic and aryl alkynes with aryl iodines afforded moderate to excellent yields (Scheme 3). The reaction of iodobenzene with phenylacetylene and 1-hexyne gave the products with 97 and 90%, respectively (Table 2, entries 1 and 2). Aryl iodides bearing an electron-donating group were less reactive. The cross-coupling of 4-methoxy and 3-methyl iodobenzene gave 57−78% (Table 2, entries 3−5) and 62−86% (Table 2, entries 10,11,17−20), respectively. To our delight, NO_2- group was tolerant, and corresponding alkynes were isolated with 65−90% yields (Table 2, entries 6−9). The sterically hindered group did not inhibit the coupling reactions. 2-CF_3−iodobenzene coupling coupled with alkynes yields were 64−78% (Table 2, entries 13−16).

3.3. Surface Characterization and Proposed Catalytic Mechanism of MMT@Pd/Cu Alloy. The interaction of heterogeneous catalysts and substrates essentially happen on the surface of the active sites. To rationalize the catalytic activity of MMT@Pd/Cu, we studied the surface features of Pd/Cu alloy and the corresponding monometallic nanoparticles with in situ FT-IR and XPS analysis. CO as molecular probe has been extensively applied for evaluating the electron-density of a

Table 2. MMT@Pd/Cu Catalyzed Cross-Coupling of Aryl Iodides and Alkynes[a]

entry	R_1	R_2	product	yield[b]
1	H	C_6H_5	3	97
2	H	n-C_6H_{13}	4	90
3	4-CH_3O	n-C_4H_9	5	67
4	4-CH_3O	n-C_6H_{13}	6	78
5	4-CH_3O	n-C_4H_9	7	57
6	4-NO_2	n-C_4H_9	8	90
7	3-NO_2	n-C_4H_9	9	70
8	4-NO_2	n-C_4H_9	10	65
9	3-NO_2	n-C_6H_{13}	11	73
10	3-CH_3	n-C_4H_9	12	62
11	3-CH_3	n-C_6H_{13}	13	75
12	H	4-$C_2H_5C_6H_5$	14	85
13	2-CF_3	4-$CH_3C_6H_4$	15	68
14	2-CF_3	C_6H_5	16	72
15	2-CF_3	4-$C_2H_5C_6H_5$	17	64
16	2-CF_3	4-$C_5H_{11}C_6H_5$	18	78
17	3-CH_3	C_6H_5	19	80
18	3-CH_3	4-$C_2H_5C_6H_4$	20	63
19	3-CH_3	4-$C_5H_{11}C_6H_4$	21	77
20	3-CH_3	4-$CH_3C_6H_4$	22	86

[a]Reaction conditions: MMT@Pd/Cu (Pd 1 mol %); K_2CO_3, 1.0 mmol; absolute ethanol 5 mL; PPh_3 2.0 mol %; PhR_1 1.0 mmol; PhC≡CHR_2 1.0 mmol; temperature, 65 °C; in N_2; 16 h. [b]Percent yields after isolated by silica column chromatography.

Scheme 3. MMT@Pd/Cu Catalyzed Cross-Coupling of Aryl Iodides and Alkynes

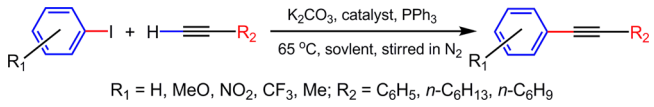

transition metal catalyst.[28] In a vacuum chamber containing the self-support disk of MMT@M, 99.99% CO (0.07 Torr) was filled and kept for an appropriate amount of time. After the absorbed CO was removed, in situ FT-IR spectra of the MMT@M showed CO bonded to the corresponding metallic sites (Figure 6). Two carbonyl absorptions at 2133 and 2070 cm^{-1} were assigned as Cu(I)−CO[29] and Cu(0)−CO,[30] according to literature values. CO on MMT@Pd (Figure 6b, red curve) showed two absorptions at 2125 and 2179 cm^{-1}, which can be attributed terminal bonded carbonyls to Pd^0 [31] and Pd^{2+},[32] respectively. The comparison of CO adsorption of MMT@Pd/Cu with monometallic MMT revealed that Pd−CO and Cu−CO of Pd/Cu alloy slightly red-shifts to 2119 and 2063 cm^{-1}. These observations can be rationalized as more back-donation of d-electron from alloy particles to CO, indicating higher activity of both palladium and copper for

Table 1. MMT-Supported Metals Catalyzed Sonogashira Reactions[a]

entry	catalyst	yield[b]	entry	catalyst	yield[b]
1	MMT@Pd	32	6	MMT@Pd/Fe	6
2	MMT@Cu	40	7	MMT@Pd/Cu	97
3	MMT@Fe	23	8	Pd@MMT+CuI	30
4	MMT@Ni	17	9	Cu@MMT+Pd(OAc)$_2$	10
5	MMT@Pd/Ni	28	10	Pd@MMT+Cu@MMT	26

[a]Reaction conditions: 1 mmol PhI; 1 mmol PhC≡CH; 1 mmol catalyst, Pd, 1 mol %; 1 mmol K_2CO_3; 5 mL of ethanol; 2 mol % PPh_3. [b]Isolated yields.

dx.doi.org/10.1021/am505798y | ACS Appl. Mater. Interfaces 2014, 6, 20261−20268

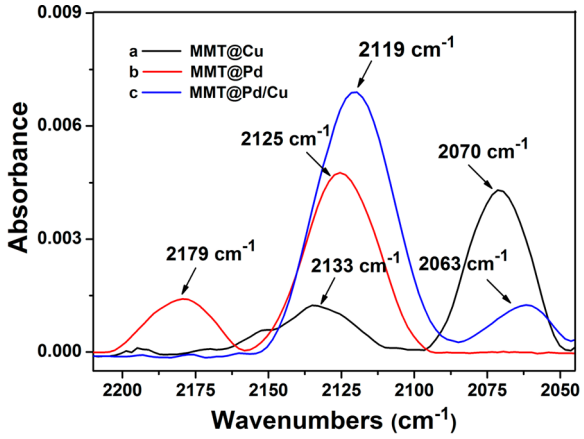

Figure 6. In situ FT-IR spectra of CO adsorbed on MMT@M (M = Pd, Cu): (a) MMT@ Cu, (b) MMT@Pd, and (c) MMT@Pd/Cu.

the cross-coupling reactions. It was found that Pd in Pd/Cu bimetallic NPs existed both zerovalent and divalent while Cu had monovalence.

The valence state of Pd/Cu alloy were analyzed by XPS. Figure 7 showed the XPS core level spectra for Pd 3d, which were characterized by spin−orbit splitting (Pd $3d_{5/2}$ and Pd $3d_{3/2}$ components). Notably, an approximately 0.1−0.3 eV chemical shift of the Cu 2p and Pd 3d core level was observed in the standard Pd and Cu samples. In Figure 7a, the peaks corresponding to Pd $3d_{5/2}$ and Pd $3d_{5/2}$ appeared at 337.9 and 342.8 eV, respectively. The Pd($3d_{5/2, 3/2}$) peaks at 340.4 and 335.1 eV were assigned to Pd^0.[33] Figure 7b shows the Cu 2p core level XPS spectra, in which a Cu $2p_{3/2}$ peak at 932.2 eV corresponding to Cu^+ was evident, accompanied by peaks centered at 950.0 eV due to spin−orbit coupling of Cu^0.[34] Therefore, the fact that no Cu^{2+} signal was present in the XPS spectra suggested that all Cu^{2+} precursors were reduced to low valence copper species under these conditions. Overall, XPS analyses were in agreement with the ones from in situ IR analyses, indicating that unique Pd/Cu alloy moieties were formed in the MMT@Pd/Cu material.

Pd/Cu catalyst system have been extensively applied for Sonogashira couplings, however, the true catalytic species are not clearly understood. In a well-accepted catalytic cycle,[33] Pd(0) is responsible for activating Sp^2C−X bond and Cu(I) form metalacetylide with terminal alkyne. The acetylide moiety transmetalated to Pd, and the reductive elimination released the cross-coupling product. Pd(0) and Cu(I) cooperatively catalyze the reaction in two different cycles. Our catalytic experimentations clearly demonstrated that Pd/Cu alloy exhibited the highest activity (Table 1, entry 7; Figure S7, Supporting Information). The observation indicated that nanoalloy might be a true active species in an efficient Pd/Cu catalyst system. Without the formation of nanoalloy, bimetallic catalyst that even consisted of palladium and copper cannot catalyze the cross-coupling reaction (Table 1, entries 8−10; Figure S7, Supporting Information). Therefore, the catalytic synergistic effect of bimetallic alloy was proposed in this case.

In MMT@Pd/Cu catalyzed Sonogashira coupling reaction, Pd/Cu nanoalloy were released from the MMT layer and readily stabilized by PPh_3. Then, the oxidative addition reaction occurred between PhI and palladium atoms of nanoalloy while copper coordinated to phenylacetylene via π-donating bonding. After HI was removed by the base, aryl-Pd and PhCC-Cu formed consecutively. The further transmetalation process happened between adjacent palladium and copper, which should be far more efficient than the intermolecular transmetalations of the known catalytic cycle. Finally, the reductive elimination to form the cross-coupled product and regenerate the Pd/Cu nanoalloy for the next catalytic cycle.

4. CONCLUSION

In summary, we developed a facile, one-pot synthesis of MMT-supported transition metal nanoalloy. The size, distribution, composition, and surface features were studied with TEM, EDS, XRD, in situ CO absorbed IR, and XPS analyses. The nanoalloys possess narrow size distribution and well-controlled compositions. Pd and Cu sites in MMT@Pd/Cu were more electronegative than those of MMT@Pd and MMT@Cu. The catalytic properties of nanoalloy for Sonogashira reactions were examined as well, and the MMT@Pd/Cu material has exhibited catalytic activity superior to MMT@Pd and MMT@Cu. These results are consistent with the increase of electronegativity observed in Pd^0 and Cu^+ species, which probably stems from the positive synergistic effect of Pd and Cu. No synergistic effect was observed in the MMT@Pd/Ni and MMT@Pd/Fe systems. Therefore, the presence of synergistic effect could be solely dependent on the nature of metal elements. Due to the unique interaction between metallic ions, the bimetallic NPs have exhibited physicochemical properties distinctively advantageous over the monometallic NPs, which would make such materials applicable in diverse fields such as catalysis, materials science, and organic synthesis. Further studies to prepare more

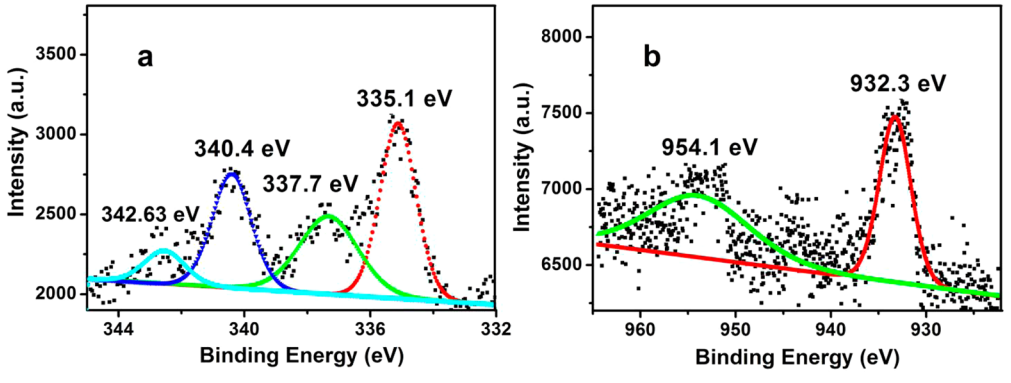

Figure 7. Core−shell XPS spectra of (a) Pd 3d and (b) Cu 2p.

bimetallic NPs and expand the scope of their applications are currently underway in our laboratory.

■ ASSOCIATED CONTENT

Supporting Information

Preparation, characterization, and analysis of MMT-supported monometallic and bimetallic transition metal nanoparticles. This material is available free of charge via the Internet at http://pubs.acs.org.

■ AUTHOR INFORMATION

Corresponding Authors

*E-mail: zwgao@snnu.edu.cn.

*E-mail: zwq@snnu.edu.cn.

Notes

The authors declare no competing financial interest.

■ ACKNOWLEDGMENTS

This work was supported by the 111 Project (B14041), the Innovative Research Team in University of China (IRT1070), the National Natural Science Foundation of China (21171112, 21271124, 21371112), the Fundamental Doctoral Fund of the Ministry of Education of China (20120202120005), the Shaanxi Innovative Team of Key Science and Technology (2013KCT-17), and the Natural Science Basic Research Plan in Shaanxi Province of China (2012JM2006). We also thank Prof. X. X. Wang, Prof. J. Yang, and Prof. Y. L. Tang for helpful discussions.

■ REFERENCES

(1) Smith, A. M.; Whyman, R. Review of Methods for the Catalytic Hydrogenation of Carboxamides. *Chem. Rev.* **2014**, *114*, 5477−5510.

(2) Yu, W. T.; Porosoff, M. D.; Chen, J. G. G. Review of Pt-Based Bimetallic Catalysis: From Model Surfaces to Supported Catalysts. *Chem. Rev.* **2012**, *112*, 5780−5817.

(3) Chen, A.; Holt-Hindle, P. Platinum-Based Nanostructured Materials: Synthesis, Properties, and Applications. *Chem. Rev.* **2010**, *110*, 3767−3804.

(4) Bianchini, C.; Shen, P. K. Palladium-Based Electrocatalysts for Alcohol Oxidation in Half Cells and in Direct Alcohol Fuel Cells. *Chem. Rev.* **2009**, *109*, 4183−4206.

(5) Mallat, T.; Baiker, A. Oxidation of Alcohols with Molecular Oxygen on Solid Catalysts. *Chem. Rev.* **2004**, *104*, 3037−3058.

(6) Zhang, P.; Li, R.; Huang, Y. M.; Chen, Q. W. A Novel Approach for the in Situ Synthesis of Pt−Pd Nanoalloys Supported on Fe_3O_4@C Core−Shell Nanoparticles with Enhanced Catalytic Activity for Reduction Reactions. *ACS Appl. Mater. Interfaces* **2014**, *6*, 2671−2678.

(7) Sengupta, D.; Saha, J.; De, G.; Basu, B. Pd/Cu Bimetallic Nanoparticles Embedded in Macroporous Ion-Exchange Resins: An Excellent Heterogeneous Catalyst for the Sonogashira Reaction. *J. Mater. Chem. A* **2014**, *2*, 3986−3992.

(8) Ma, J.; Huang, X.; Liao, X. P.; Shi, B. Preparation of Highly Active Heterogeneous Au@Pd Bimetallic Catalyst Using Plant Tannin Grafted Collagen Fiber as the Matrix. *J. Mol. Catal. A: Chem.* **2013**, *366*, 8−16.

(9) Zhang, L. F.; Zhong, S. L.; Xu, A. W. Highly Branched Concave Au/Pd Bimetallic Nanocrystals with Superior Electrocatalytic Activity and Highly Efficient SERS Enhancement. *Angew. Chem., Int. Ed.* **2013**, *52*, 645−649.

(10) Paunovic, P.; Oedomsky, V.; D'Angelo, M. F. N.; Schouten, J. C.; Nijhuis, A. T. Direct Synthesis of Hydrogen Peroxide Over Au−Pd Catalyst in a Wall-Coated Microchannel. *J. Catal.* **2014**, *309*, 325−332.

(11) Wang, L.; Nemoto, Y.; Yamauchi, Y. Direct Synthesis of Spatially-Controlled Pt-on-Pd Bimetallic Nanodendrites with Superior Electrocatalytic Activity. *J. Am. Chem. Soc.* **2011**, *133*, 9674−9677.

(12) Wang, L.; Yamauchi, Y. Metallic Nanocages: Synthesis of Bimetallic Pt−Pd Hollow Nanoparticles with Dendritic Shells by Selective Chemical Etching. *J. Am. Chem. Soc.* **2013**, *135*, 16762−16765.

(13) Fox, E. B.; Velu, S.; Engelhard, M. H.; Chin, Y. H.; Miller, J. T.; Kropf, J.; Song, C. S. Characterization of CeO_2-Supported Cu−Pd Bimetallic Catalyst for the Oxygen-Assisted Water−Gas Shift Reaction. *J. Catal.* **2008**, *260*, 358−370.

(14) Han, Y. X.; Peng, D.; Xu, Z. Y.; Wan, H. H.; Zheng, S. R.; Zhu, D. Q. TiO_2 Supported Pd@Ag as Highly Selective Catalysts for Hydrogenation of Acetylene in Excess Ethylene. *Chem. Commun.* **2013**, *49*, 8350−8352.

(15) Slanac, D. A.; Hardin, W. G.; Johnston, K. P.; Stevenson, K. J. Atomic Ensemble and Electronic Effects in Ag-Rich AgPd Nanoalloy Catalysts for Oxygen Reduction in Alkaline Media. *J. Am. Chem. Soc.* **2012**, *134*, 9812−9819.

(16) Yin, Z.; Zhou, W.; Gao, Y. J.; Ma, D.; Kiely, C. J.; Bao, X. H. Supported Pd−Cu Bimetallic Nanoparticles That Have High Activity for the Electrochemical Oxidation of Methanol. *Chem.—Eur. J.* **2012**, *18*, 4887−4893.

(17) Kariuki, N. N.; Wang, X. P.; Mawdsley, J. R.; Ferrandon, M. S.; Niyogi, S. G.; Vaughey, J. T.; Myers, D. J. Colloidal Synthesis and Characterization of Carbon-Supported Pd−Cu Nanoparticle Oxygen Reduction Electrocatalysts. *Chem. Mater.* **2010**, *22*, 4144−4152.

(18) Wallis, P. J.; Chaffee, A. L.; Gates, W. P.; Patti, A. F.; Scott, J. L. Partial Exchange of Fe(III) Montmorillonite with Hexadecyltrimethylammonium Cation Increases Catalytic Activity for Hydrophobic Substrates. *Langmuir* **2010**, *26*, 4258−4265.

(19) Chinchilla, R.; Nájera, C. The Sonogashira Reaction: A Booming Methodology in Synthetic Organic Chemistry. *Chem. Rev.* **2007**, *107*, 874−922.

(20) Chinchilla, R.; Nájera, C. Recent Advances in Sonogashira Reactions. *Chem. Soc. Rev.* **2011**, *40*, 5084−5121.

(21) Enache, D. I.; Edwards, J. K.; Landon, P.; Solsona, B. E.; Carley, A. F.; Herzing, A. A.; Watanabe, M.; Kiely, C. J.; Knight, D. W.; Hutchings, G. J. Solvent-Free Oxidation of Primary Alcohols to Aldehydes Using Au-Pd/TiO_2 Catalysts. *Science* **2006**, *311*, 362−365.

(22) Liu, X. Y.; Wang, A. Q.; Li, L.; Zhang, T.; Moub, C. Y.; Lee, J. F. Structural Changes of Au−Cu Bimetallic Catalysts in CO Oxidation: In situ XRD, EPR, XANES, and FT-IR Characterizations. *J. Catal.* **2011**, *278*, 288−296.

(23) Xu, W.; Sun, Y. L.; Guo, M. H.; Zhang, W. Q.; Gao, Z. W. Montmorillonite Supported Pd/Cu Bimetallic Nanoparticles Catalyzed Sonogashria Coupling. *Chin. J. Org. Chem.* **2013**, *33*, 820−826.

(24) Park, S. B.; Alper, H. Recyclable Sonogashira Coupling Reactions in an Ionic Liquid, Effected in the Absence of Both a Copper Salt and a Phosphine. *Chem. Commun.* **2004**, 1306−1307.

(25) Gao, S. X.; Zhao, N.; Shu, M. H.; Che, S. A. Palladium Nanoparticles Supported on MOF-5: A Highly Active Catalyst for a Ligand- and Copper-Free Sonogashira Coupling Reaction. *Appl. Catal., A* **2010**, *388*, 196−201.

(26) Roucoux, A.; Schulz, J.; Patin, H. Reduced Transition Metal Colloids: A Novel Family of Reusable Catalysts? *Chem. Rev.* **2002**, *102*, 3757−3778.

(27) Hong, F.; Sun, S. D.; You, H. J.; Yang, S. C.; Fang, J. X.; Guo, S. W.; Yang, Z. M.; Ding, B. J.; Song, X. P. Cu_2O Template Strategy for the Synthesis of Structure-Definable Noble Metal Alloy Mesocages. *Cryst. Growth Des.* **2011**, *11*, 3694−3697.

(28) Chopra, I. S.; Chaudhuri, S.; Veyan, J. F.; Chabal, Y. J. Turning Aluminium into a Noble-Metal-Like Catalyst for Low-Temperature Activation of Molecular Hydrogen. *Nat. Mater.* **2011**, *10*, 884−889.

(29) Hadjiivanov, K.; Knözinger, H. FT-IR Study of CO and NO Adsorption and Coadsorption on a Cu/SiO_2 Catalyst: Probing the Oxidation State of Copper. *Phys. Chem. Chem. Phys.* **2001**, *3*, 1132−1137.

(30) Bautista, F. M.; Blanco, A.; Campelo, J. M.; Garcia, A.; Luna, D.; Marinas, J. M.; Romero, A. A. Continuous Flow Toluene Methylation over $AlPO_4$ and $AlPO_4$−Al_2O_3 Catalysts. *Catal. Lett.* **1994**, *29*, 159−167.

(31) Hess, C.; Ozensoy, E.; Goodman, D. W. Combined in Situ Infrared and Kinetic Study of the Catalytic CO + NO Reaction on Pd(111) at Pressures up to 240 mbar. *J. Phys. Chem. B* **2003**, *107*, 2759−2764.
(32) Belskaya, O. B.; Danilova, I. G.; Kazakov, M. O.; Mironenko, R. M.; Lavrenov, A. V.; Likholobov, V. A. In *Infrared Spectroscopy—Materials Science, Engineering and Technology*. Theophanides, T., Ed.; InTech: Rijeka, Croatia, 2012; Chapter 7, pp 150−178.
(33) Colón, G.; Maicu, M.; Hidalgo, M. C.; Navío, J. A. Cu-Doped TiO_2 Systems with Improved Photocatalytic Activity. *Appl. Catal., B* **2006**, *67*, 41−51.
(34) Thathagar, M. B.; Beckers, J.; Rothenberg, G. Palladium-Free and Ligand-Free Sonogashira Cross-Coupling. *Green Chem.* **2004**, *6*, 215−218.